

Efficient, scalable and solvent-free mechanochemical synthesis of the OLED material Alq₃ (q = 8-hydroxyquinolate)

Xiaohe Ma, Gin Keat Lim, Kenneth D.M. Harris, David C. Apperley, Peter N. Horton, Michael B. Hursthouse and Stuart L. James

Supporting Information

Contents:

	Page
Experimental Details	3
Table Theoretical and experimental microanalyses, and theoretical and experimental mass losses for thermogravimetric analyses	4
Single-crystal XRD Experimental Details	4
Structure Determination of Alq₃.AcOH-m Directly from Powder XRD Data	5
Figure S0 Results of (a) Le Bail fitting and (b) final Rietveld refinement for Alq ₃ .AcOH-m.	6
Figure S1 Comparison of powder XRD patterns of Alq ₃ .AcOH-m and the starting materials Al(OAc) ₂ OH and 8-hydroxyquinoline.	7
Figure S2 Solid-state ¹³ C CPMAS NMR spectrum of the starting material Al(OAc) ₂ OH.	8
Figure S3 Solid-state ²⁷ Al MAS NMR spectrum of the starting material Al(OAc) ₂ OH.	9
Figure S4 Solid-state ¹³ C CPMAS NMR spectrum of the starting material 8-hydroxyquinoline.	10
Figure S5 Solid-state ¹³ C CPMAS NMR spectrum of Alq ₃ .AcOH-m.	11
Figure S6 Solid-state ²⁷ Al MAS NMR spectrum of Alq ₃ .AcOH-m.	12
Figure S7 Comparison of the experimental solid-state ²⁷ Al MAS NMR spectrum of Alq ₃ .AcOH-m and a simulated spectrum based on a single ²⁷ Al crystallographic environment.	13
Figure S8 Solution-state ¹ H NMR spectrum of Alq ₃ .AcOH-m in CDCl ₃ .	14
Figure S9 Interaction between the Alq ₃ and acetic acid molecules in the crystal structure of Alq ₃ .AcOH-s, determined from single-crystal XRD.	15
Figure S10 Comparison of the experimental powder XRD pattern of crushed single crystals of Alq ₃ .AcOH-s and the powder XRD pattern simulated from the crystal structure of Alq ₃ .AcOH-s determined from single-crystal XRD data.	16
Figure S11 Comparison of the experimental powder XRD pattern of Alq ₃ .AcOH-m and the powder XRD pattern simulated from the crystal structure of Alq ₃ .AcOH-s determined from single-crystal XRD data.	17

Figure S12 Comparison of the experimental powder XRD patterns of Alq ₃ .AcOH- m and Alq ₃ - m .	18
Figure S13 Comparison of the experimental powder XRD pattern of Alq ₃ - m and the simulated powder XRD patterns for the known α and ϵ phases of Alq ₃ .	19
Figure S14 Solution-state ¹ H NMR spectrum of Alq ₃ .AcOH- m in CDCl ₃ .	20
Figure S15 Solid-state ¹³ C CPMAS NMR spectrum of Alq ₃ - m .	21
Figure S16 Solid-state ²⁷ Al MAS NMR spectrum of Alq ₃ - m .	22
Figure S17 SEM images of Alq ₃ .AcOH- m (above) and Alq ₃ - m (below).	23
Figure S18 Comparison of powder XRD patterns recorded for the product from the large-scale synthesis of Alq ₃ .AcOH- m from 10 min to 45 min reaction time.	24
Figure S19 Comparison of experimental powder XRD patterns of Alq ₃ .AcOH- m obtained from small-scale and large-scale syntheses.	25
Figure S20 Solution-state ¹ H NMR spectrum of Alq ₃ .AcOH- m obtained from large-scale synthesis.	26
Figure S21 Solid-state ¹³ C CPMAS NMR spectrum of Alq ₃ .AcOH- m prepared at large scale.	27
Figure S22 Solid-state ¹³ C CPMAS NMR spectrum of Alq ₃ - m prepared at large scale.	28

Experimental Details

Small-scale mechanochemical synthesis: The reaction was carried out in a Retsch MM400 shaker ball mill under ambient conditions. Basic aluminum diacetate ($\text{Al}(\text{OAc})_2\text{OH}$, 0.324 mg, 2 mmol) and 8-hydroxyquinoline ($8\text{-NC}_9\text{H}_6\text{OH}$, 0.870 mg, 6 mmol) were placed in a 20 cm^3 steel grinding jar with one 10 mm diameter steel ball which was vibrated at 25 Hz for 15 mins. The product was decanted to give $\text{Alq}_3\text{.AcOH-m}$ (1.117 g, 93.54% yield).

Large-scale mechanochemical synthesis: The reaction was carried out in a Retsch PM100 Planetary Ball Mill. Basic aluminum diacetate ($\text{Al}(\text{OAc})_2\text{OH}$, 16.2 g, 0.1 mol) and 8-hydroxyquinoline ($8\text{-NC}_9\text{H}_6\text{OH}$, 45.3 g, 0.3 mol) were placed in a 250 cm^3 steel grinding jar with 50 steel balls of 10mm diameter, which was rotated at 450 rpm for 35 mins. The product was decanted to give $\text{Alq}_3\text{.AcOH-m}$ (48.25 g, 78.46% yield).

Growth of single crystals of $\text{Alq}_3\text{.AcOH-s}$: Large single crystals were obtained from a saturated acetic acid solution of $\text{Alq}_3\text{-m}$ by layering with acetone after two weeks.

Solid-state ^{13}C NMR spectra: Spectra were recorded at 100.56 MHz using a Varian VNMRS spectrometer and either 4 mm or 6 mm (rotor o.d.) magic-angle spinning probes. The spectra were recorded using cross-polarization, with the conditions given in the figure captions, at ambient probe temperature ($\sim 25^\circ\text{C}$). Spectra are referenced with respect to an external sample of neat tetramethylsilane (carried out by setting the high-frequency signal from adamantane to 38.5 ppm).

Solid-state ^{27}Al NMR spectra: Spectra were recorded at 104.20 MHz using a Varian VNMRS spectrometer and a 4 mm (rotor o.d.) magic-angle spinning probe. The spectra were recorded using direct excitation, with the conditions given in the figure captions and at ambient probe temperature ($\sim 25^\circ\text{C}$). Spectra are referenced with respect to an external sample of 1 M aqueous $\text{Al}(\text{NO}_3)_3$.

Table Theoretical and experimental microanalyses, and theoretical and experimental mass losses for thermogravimetric analyses (TGA).

	Al%	C%	H%	N%	% mass loss
Alq ₃ (calc.)	5.88	70.59	3.92	9.15	0
Alq ₃ .AcOH (calc.)	5.20	67.05	4.23	8.09	11.56
Alq ₃ .AcOH- m	4.82	66.56	4.47	8.31	11.73
Alq ₃ .AcOH- s	–	66.89	4.85	8.02	–
Alq ₃ - m	6.24	69.68	4.46	8.89	–
Alq ₃ .AcOH- m (large scale)	–	66.77	4.73	8.17	–
Alq ₃ - m (large scale)	–	70.40	4.07	9.06	–

Single-crystal XRD Experimental Details

The single-crystal XRD data collection for Alq₃.AcOH-**s** was carried out at 120(2) K using a Nonius Kappa CCD diffractometer with MoK α radiation ($\lambda = 0.71073 \text{ \AA}$), controlled by the Collect¹ software package. The data were processed using Denzo² and semi-empirical absorption corrections were applied using SADABS.³ The structure was solved by direct methods and refined by full-matrix least-square procedures on F^2 using SHELXS-97⁴ and SHELXL-97⁴ respectively. All non-hydrogen atoms were refined anisotropically, with all hydrogen atoms placed geometrically using standard riding models.

Crystal Data for Alq₃.AcOH-**s**: C₂₉H₂₂AlN₃O₅; $M = 519.48 \text{ g mol}^{-1}$; $T = 120(2) \text{ K}$; $\lambda = 0.71073 \text{ \AA}$; Monoclinic, space group P2₁/n; $a = 11.7123(2) \text{ \AA}$, $b = 12.9534(2) \text{ \AA}$, $c = 16.5625(2) \text{ \AA}$, $\beta = 96.701(1)^\circ$; $V = 2495.60(6) \text{ \AA}^3$; $Z = 4$; $\rho_{\text{calc}} = 1.384 \text{ Mg m}^{-3}$; $\mu(\text{Mo-K}\alpha) = 0.128 \text{ mm}^{-1}$; $F(000) = 1080$; crystal size = $0.52 \times 0.40 \times 0.22 \text{ mm}^3$. A total of 30493 reflections were collected ($2.93 \leq \theta \leq 27.48^\circ$) of which 5699 reflections were independent ($R_{\text{int}} = 0.0320$). 345 parameters, $GoF = 1.046$, $R_1[|I| > 2\sigma(I_0)] = 0.0365$, $wR_2[|I| > 2\sigma(I_0)] = 0.0896$; R_1 (all reflections) = 0.0426, wR_2 (all reflections) = 0.0929; $-0.233 < \Delta\rho < 0.293 \text{ e\AA}^{-3}$.

¹ Hooft, R. *Collect, data collection software*, Nonius BV, Delft, The Netherlands, 1998.

² Otwinowski, Z.; Minor, W. *Methods Enzymol.* **1997**, *276*, 307.

³ Sheldrick, G.M. *SADABS, Program for area detector adsorption correction*, Institute for Inorganic Chemistry, University of Göttingen, Germany, 1996.

⁴ Sheldrick, G.M. *Acta Crystallogr. Sect. A* **2008**, *64*, 112.

Structure Determination of Alq₃.AcOH-m Directly from Powder XRD Data

The powder XRD pattern of Alq₃.AcOH-m was recorded at ambient temperature on a Bruker D8 powder X-ray diffractometer (CuK_{α1} radiation; Ge monochromated; transmission mode; 2θ range, 4° – 70°). The powder XRD data were indexed using the program DICVOL, giving the following unit cell with monoclinic metric symmetry: $a = 22.05 \text{ \AA}$, $b = 13.25 \text{ \AA}$, $c = 21.31 \text{ \AA}$, $\beta = 128.1^\circ$ ($V = 4895 \text{ \AA}^3$). From systematic absences, the space group was assigned as P2₁/n. Given the unit cell volume and consideration of density, the number of formula units of Alq₃.AcOH in the unit cell was assigned as $Z = 8$ (calculated density, 1.42 g cm^{-3}). Thus, for space group P2₁/n, the asymmetric unit comprises two formula units of Alq₃.AcOH ($Z' = 2$), consistent with the results from solid-state ¹³C CPMAS NMR. Unit cell and profile refinement, carried out using the Le Bail method, gave good agreement between experimental and calculated powder XRD profiles (Fig. S0; $R_{wp} = 3.02\%$, $R_p = 2.11\%$). The refined unit cell and profile parameters obtained from the Le Bail fitting procedure were used in the subsequent structure-solution calculation.

Structure solution of Alq₃.AcOH-m was carried out directly from the powder XRD data using the direct-space genetic algorithm (GA) technique implemented in the program EAGER. With two formula units of Alq₃.AcOH in the asymmetric unit, the direct-space calculation involved four rigid fragments (two Alq₃ molecules in the *mer* geometry and two AcOH molecules). Thus, the GA structure solution calculation involved 24 structural variables (three positional variables and three orientational variables for each rigid fragment in the asymmetric unit) and was carried out for 100 generations for a population of 100 trial structures, with 40 mating operations and 30 mutation operations carried out per generation. In total, 16 independent GA calculations were carried out.

The structure solution (i.e. the trial structure with lowest R_{wp} in the GA calculations) was used as the initial structural model for Rietveld refinement carried out using the GSAS program. Standard restraints were applied to bond lengths and bond angles, planar restraints were applied to the aryl rings and four common isotropic displacement parameters (U_{iso}) were refined, specifically $U_{iso}(1)$ and $U_{iso}(2)$ for all non-H atoms of the two independent Alq₃ molecules, and $U_{iso}(3)$ and $U_{iso}(4)$ for all non-H atoms of the two independent AcOH molecules. H atoms were added according to standard geometries and the U_{iso} value for each H atom was set equal to 1.2 times the refined common U_{iso} value for the non-H atoms of the same molecule.

The final Rietveld refinement gave good agreement between experimental and calculated powder XRD patterns (Fig. S0; $R_{wp} = 5.39\%$, $R_p = 3.77\%$), with the following refined parameters: $a = 21.9948(16) \text{ \AA}$, $b = 13.1962(14) \text{ \AA}$, $c = 21.2276(15) \text{ \AA}$, $\beta = 128.0685(33)^\circ$; $V = 4850.6(8) \text{ \AA}^3$; $U_{iso}(1) = 0.065(11) \text{ \AA}^2$; $U_{iso}(2) = 0.022(9) \text{ \AA}^2$; $U_{iso}(3) = 0.057(19) \text{ \AA}^2$; $U_{iso}(4) = 0.147(24) \text{ \AA}^2$ [2θ range, 4° – 70°; 3867 profiles points; 419 refined variables].

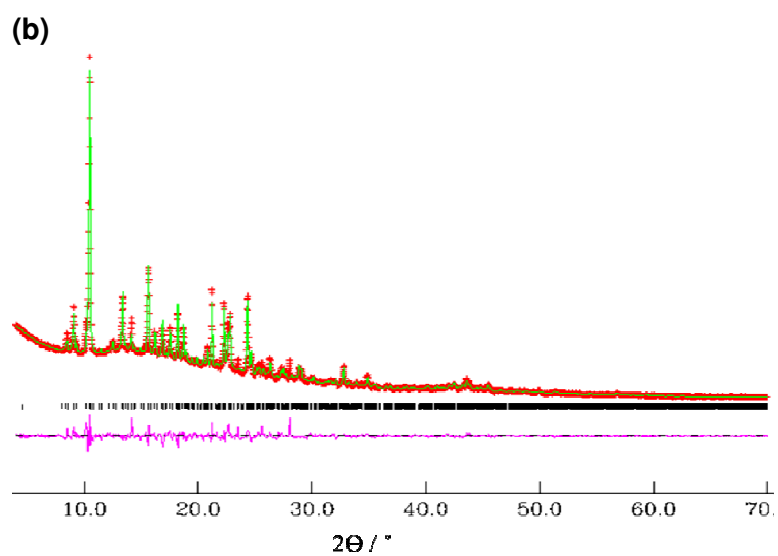
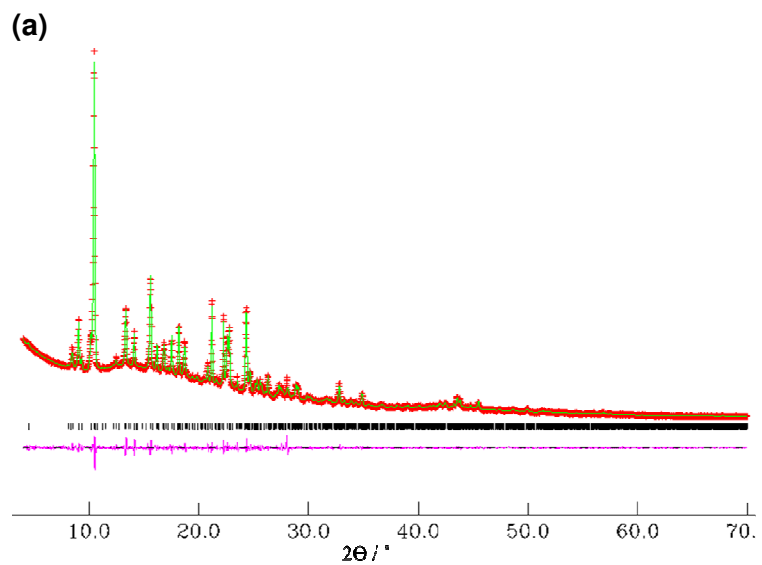


Figure S0 Results of (a) Le Bail fitting and (b) final Rietveld refinement for $\text{Alq}_3\cdot\text{AcOH-m}$, showing the experimental (+ marks), calculated (solid line) and difference (lower line) powder XRD profiles. Tick marks indicate peak positions.

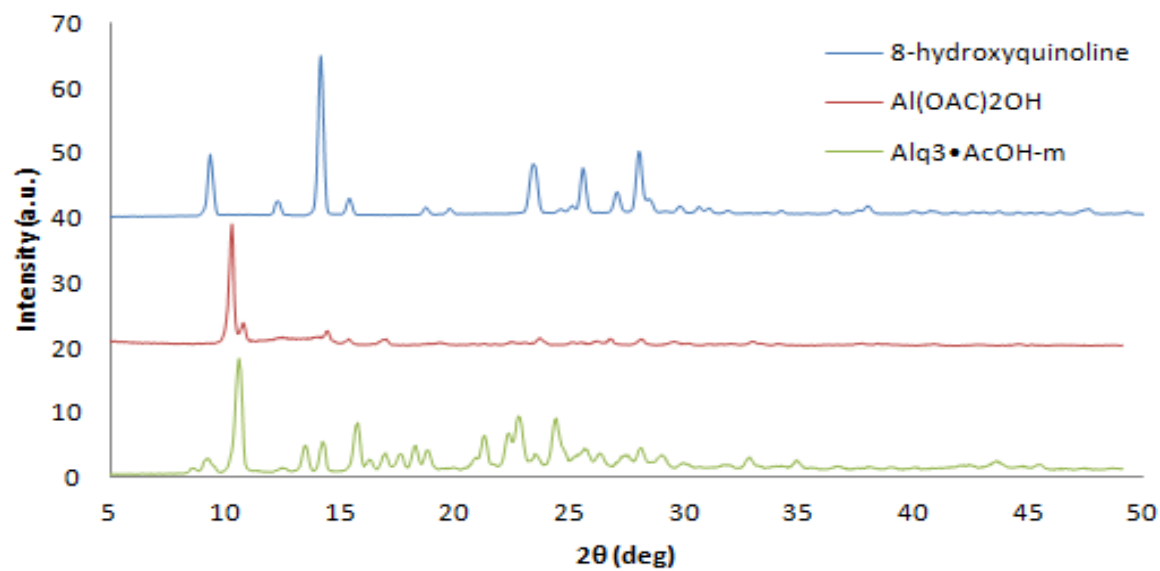


Figure S1 Comparison of powder XRD patterns of $\text{Alq}_3 \cdot \text{AcOH-m}$ and the starting materials $\text{Al}(\text{OAc})_2\text{OH}$ and 8-hydroxyquinoline.

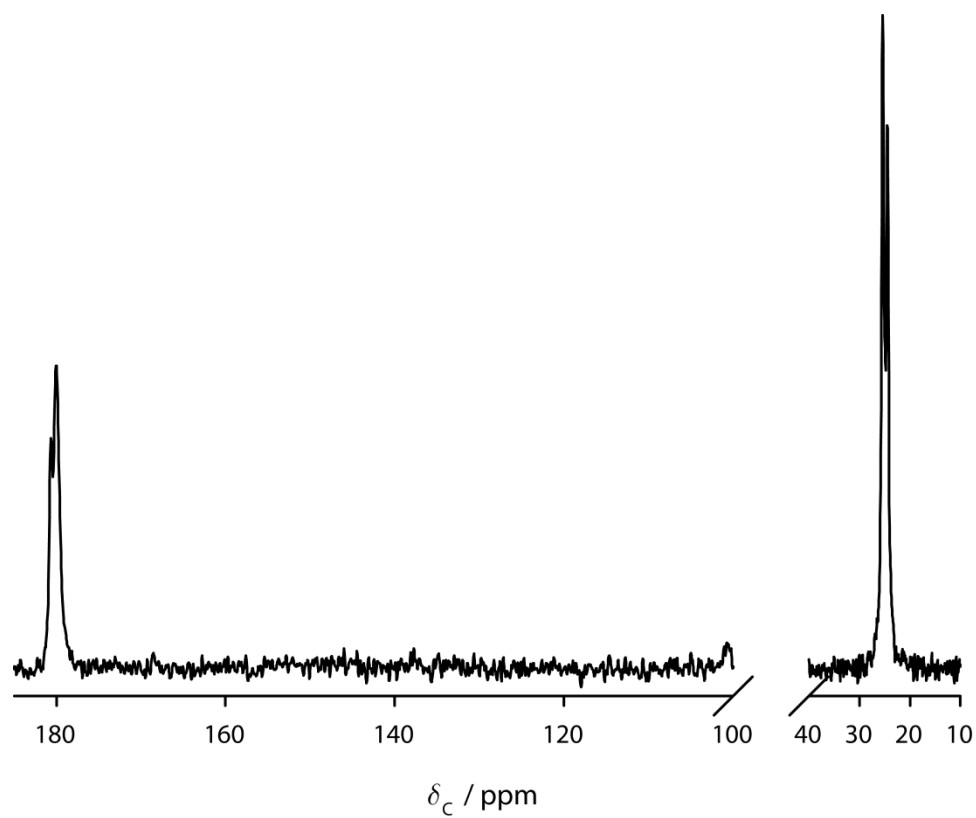


Figure S2 Solid-state ^{13}C CPMAS NMR spectrum of the starting material $\text{Al}(\text{OAc})_2\text{OH}$ (660 repetitions, 2 s recycle delay, 1 ms contact time, 8 kHz MAS frequency).

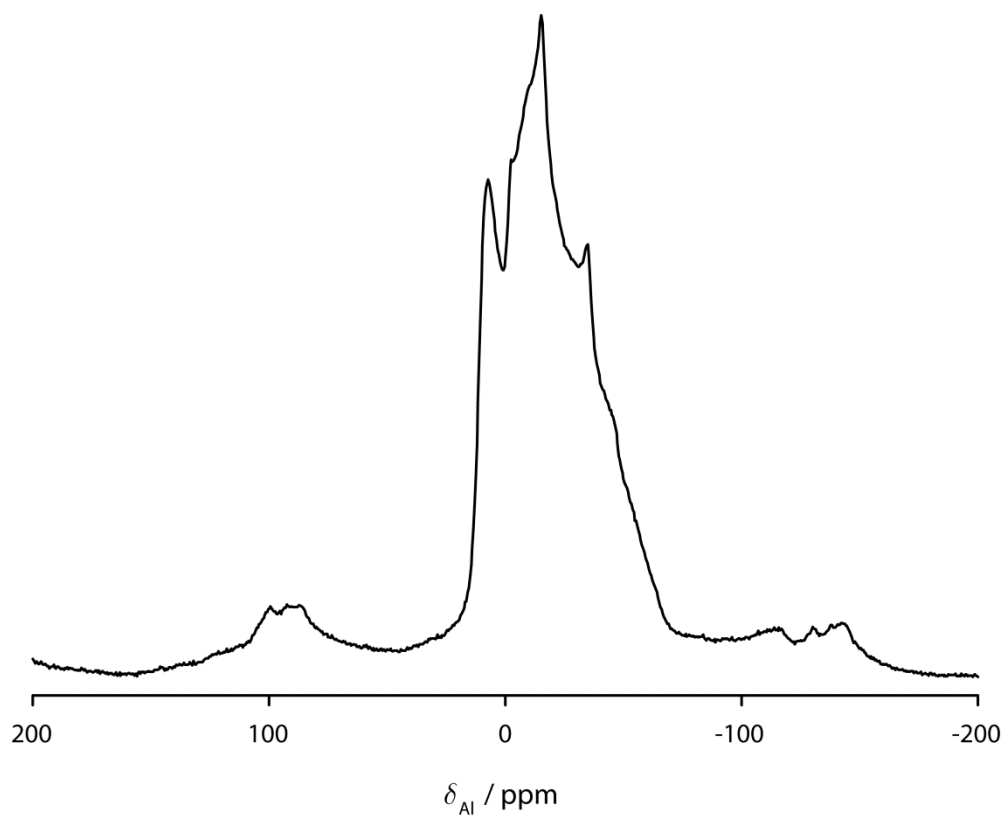


Figure S3 Solid-state ^{27}Al MAS NMR spectrum of the starting material $\text{Al}(\text{OAc})_2\text{OH}$ (11400 repetitions, 20° pulse, 0.1 s recycle delay, 12 kHz MAS frequency).

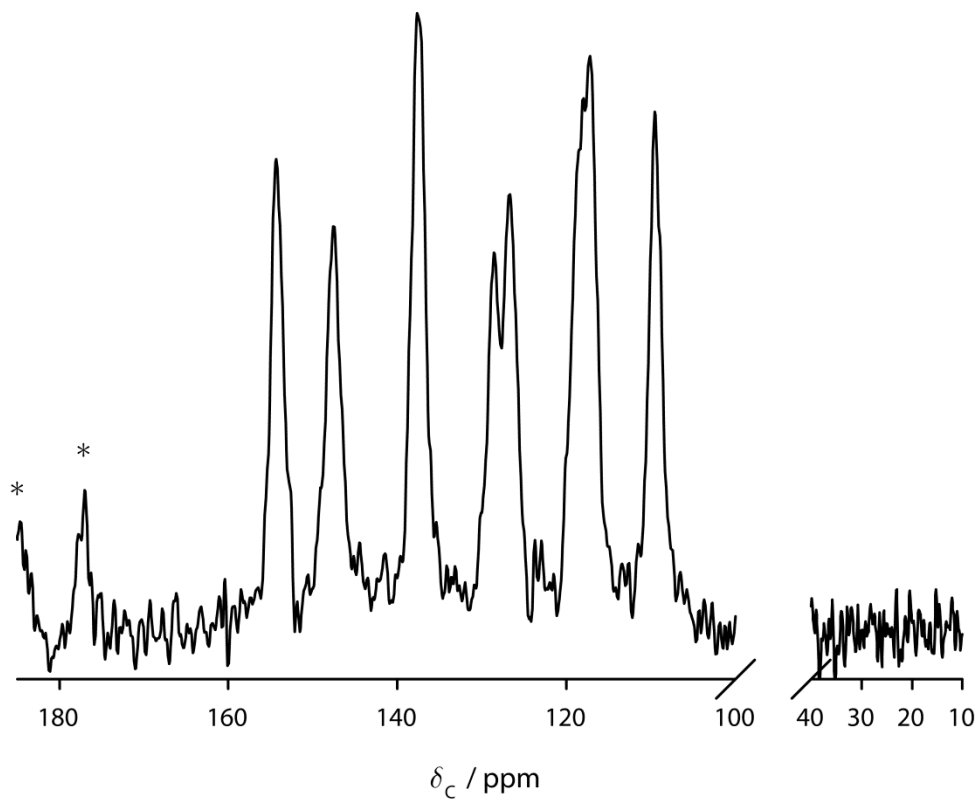


Figure S4 Solid-state ^{13}C CPMAS NMR spectrum of the starting material 8-hydroxyquinoline (17 repetitions, 300 s recycle delay, 1 ms contact time, 6.8 kHz MAS frequency). Spinning sidebands are indicated by asterisks.

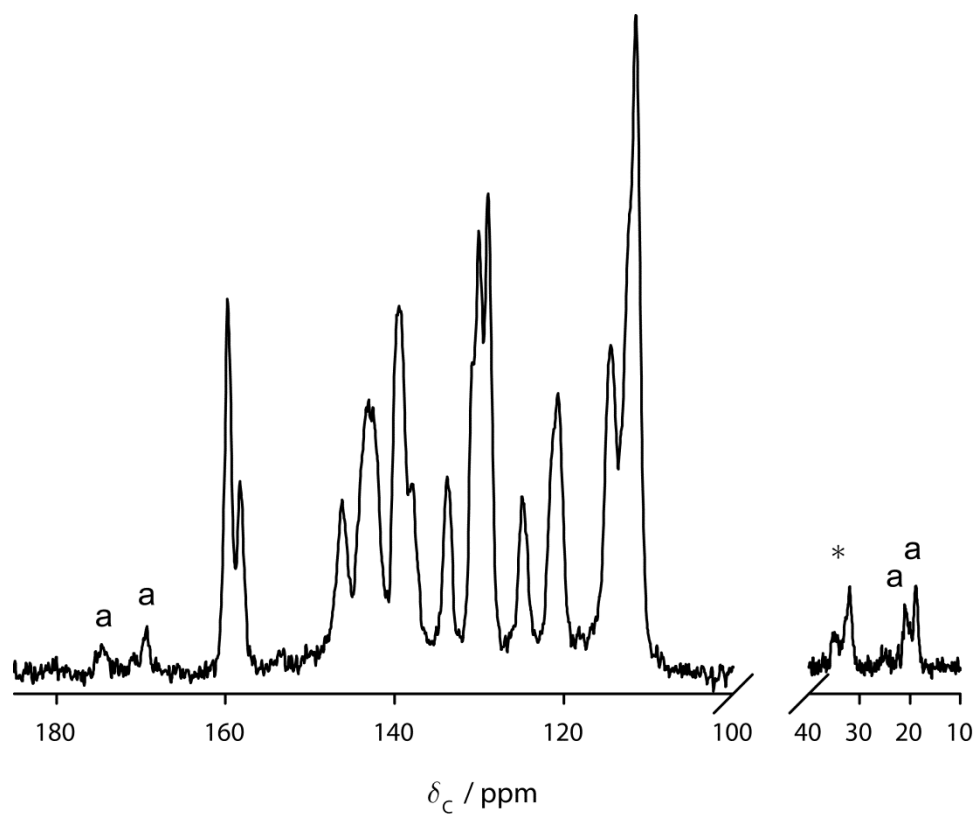


Figure S5 Solid-state ^{13}C CPMAS NMR spectrum of $\text{Alq}_3\cdot\text{AcOH}\cdot\mathbf{m}$ with COOH groups for co-crystallized acetic acid at 174.7 and 169.3 ppm (1032 repetitions, 2 s recycle delay, 1 ms contact time, 8 kHz MAS frequency). Peaks due to acetic acid are labeled “a”, and spinning sidebands are indicated by asterisks.

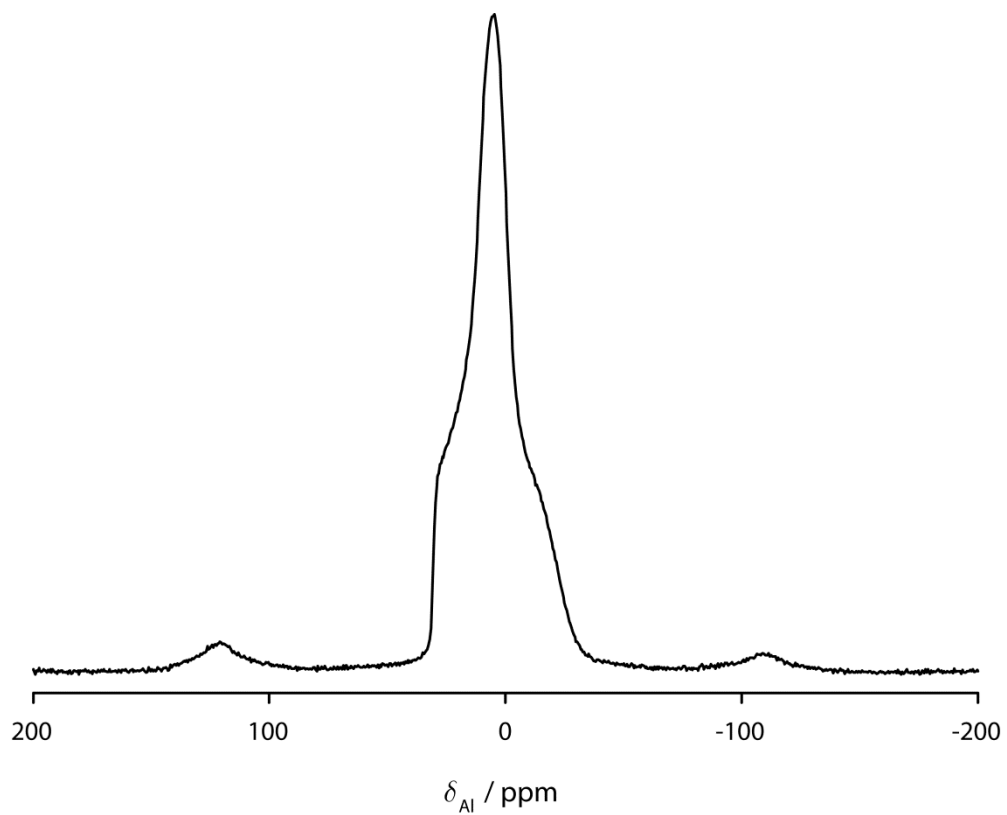


Figure S6 Solid-state ^{27}Al MAS NMR spectrum of $\text{Alq}_3\cdot\text{AcOH}\cdot\mathbf{m}$ (3800 repetitions, 20° pulse, 0.1 s recycle delay, 12 kHz MAS frequency).

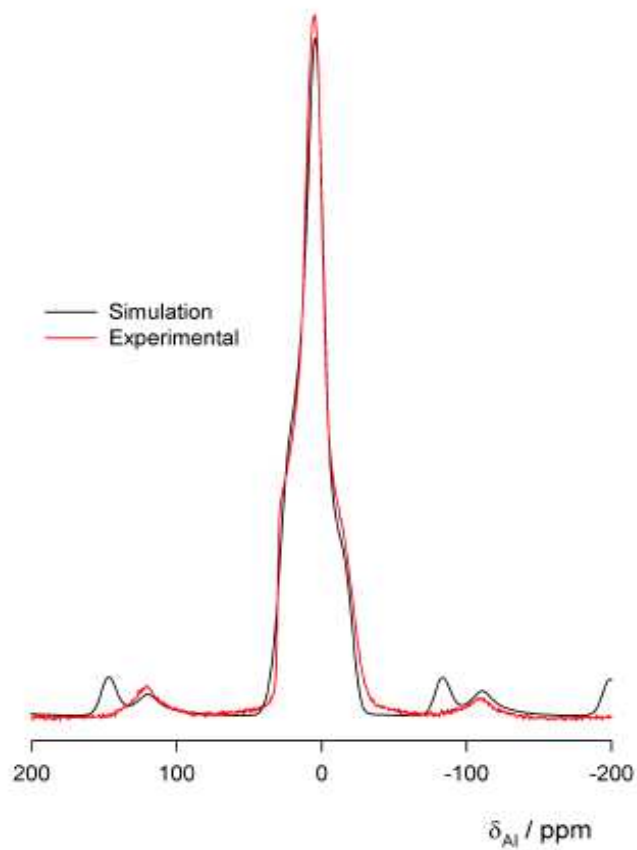


Figure S7 Comparison of the experimental solid-state ^{27}Al MAS NMR spectrum of $\text{Alq}_3\cdot\text{AcOH}\cdot\mathbf{m}$ and a simulated spectrum based on a single ^{27}Al crystallographic environment ($\delta_{\text{iso}} = 28.5$ ppm, $C_q = 5.6$ MHz, $\eta = 1.0$).

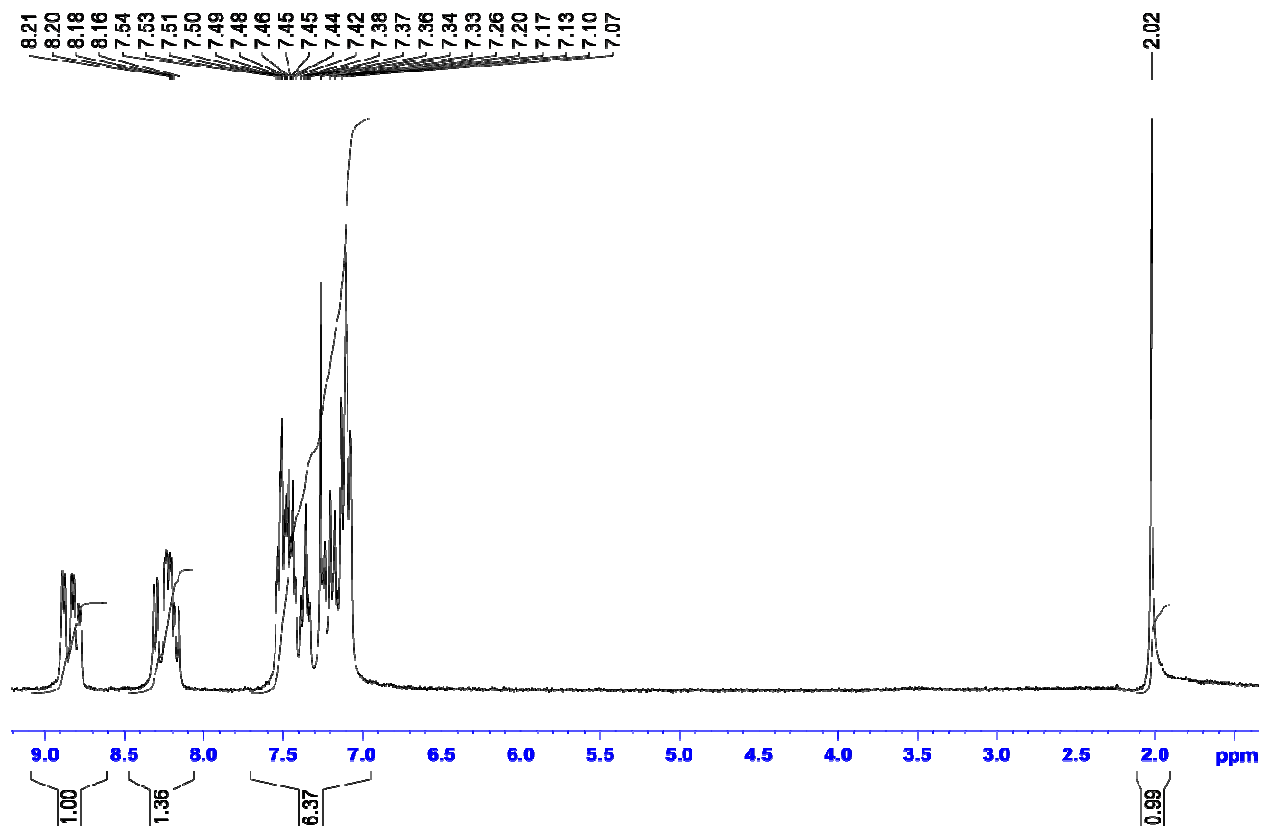


Figure S8 Solution-state ^1H NMR spectrum of $\text{Alq}_3\cdot\text{AcOH-m}$ in CDCl_3 showing the signal due to co-crystallized acetic acid at 2.02 ppm. However, we note that speciation is complicated, as some free ligand is identified from the aromatic region, suggesting that metal coordination by AcOH/AcO^- may occur in solution.

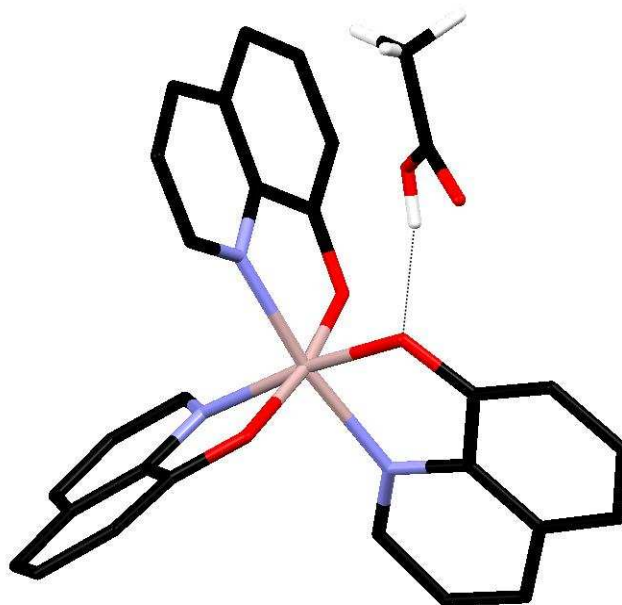


Figure S9 Interaction between the Alq₃ and acetic acid molecules in the crystal structure of Alq₃.AcOH-**s**, determined from single-crystal XRD. Hydrogen atoms of the quinolinate ligands are omitted for clarity.

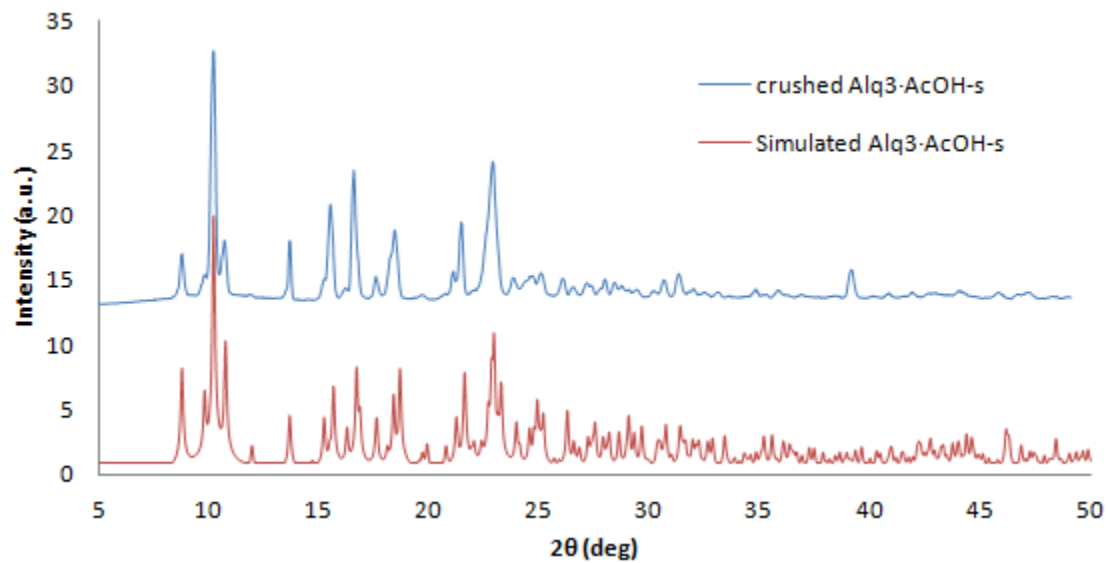


Figure S10 Comparison of the experimental powder XRD pattern of crushed single crystals of $\text{Alq}_3\cdot\text{AcOH-s}$ and the powder XRD pattern simulated from the crystal structure of $\text{Alq}_3\cdot\text{AcOH-s}$ determined from single-crystal XRD data.

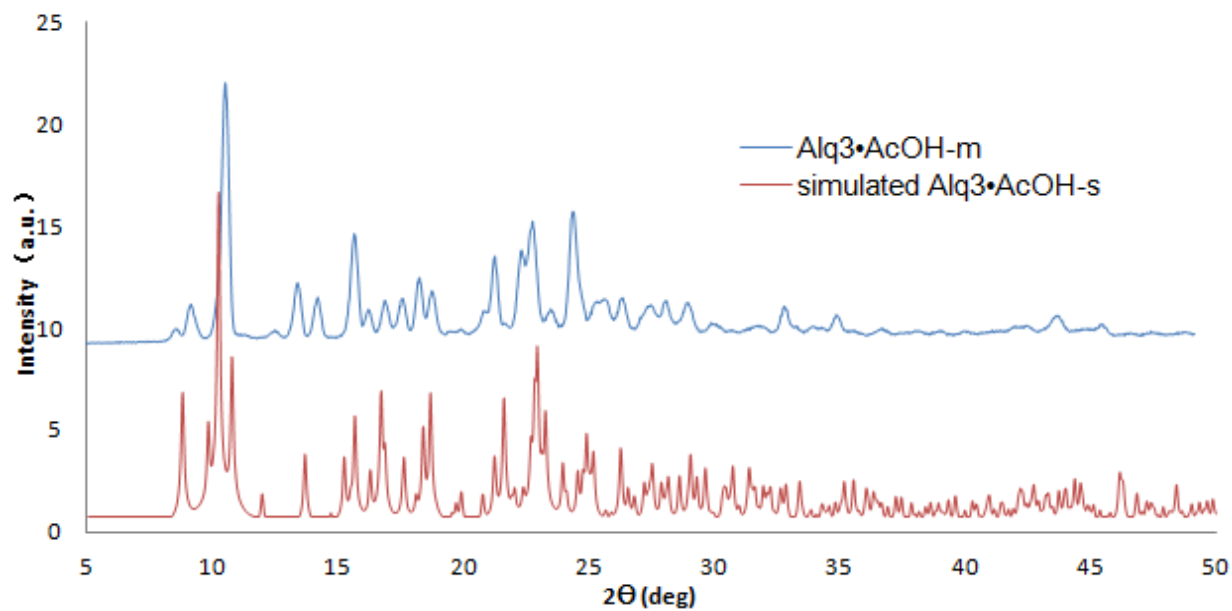


Figure S11 Comparison of the experimental powder XRD pattern of Alq₃·AcOH-**m** and the powder XRD pattern simulated from the crystal structure of Alq₃·AcOH-**s** determined from single-crystal XRD data.

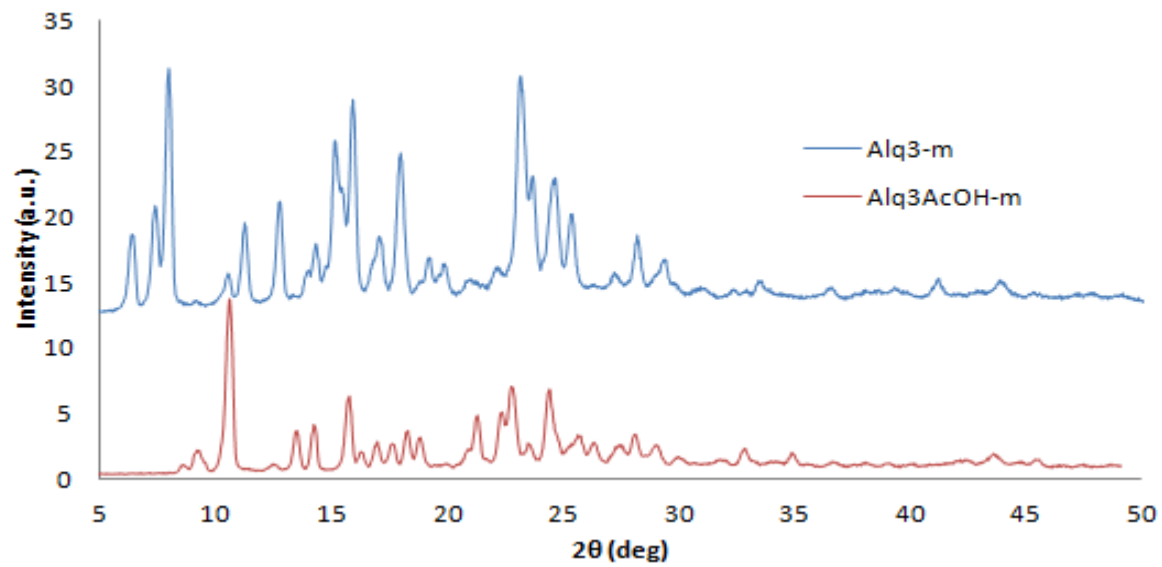


Figure S12 Comparison of the experimental powder XRD patterns of $\text{Alq}_3\cdot\text{AcOH}\cdot\mathbf{m}$ and $\text{Alq}_3\cdot\mathbf{m}$.

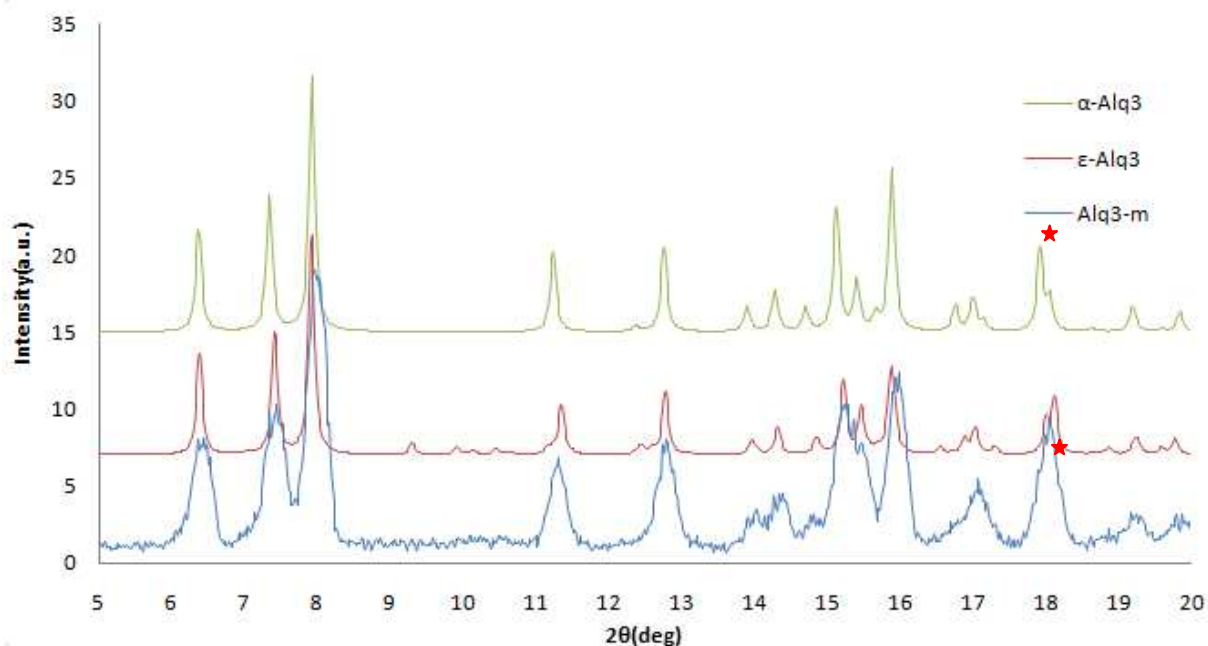


Figure S13 Comparison of the experimental powder XRD pattern of Alq₃-**m** and the simulated powder XRD patterns of the known α and ϵ phases of Alq₃ (simulated from the known crystal structures in the Cambridge Structural Database; codes QATMON01 and QATMON03 respectively). The powder XRD patterns of the α and ϵ phases of Alq₃ are very similar to each other, but the peak at $2\theta \approx 18^\circ$ in the pattern for Alq₃-**m** (indicated by a star) is taken to be diagnostic of the α phase.

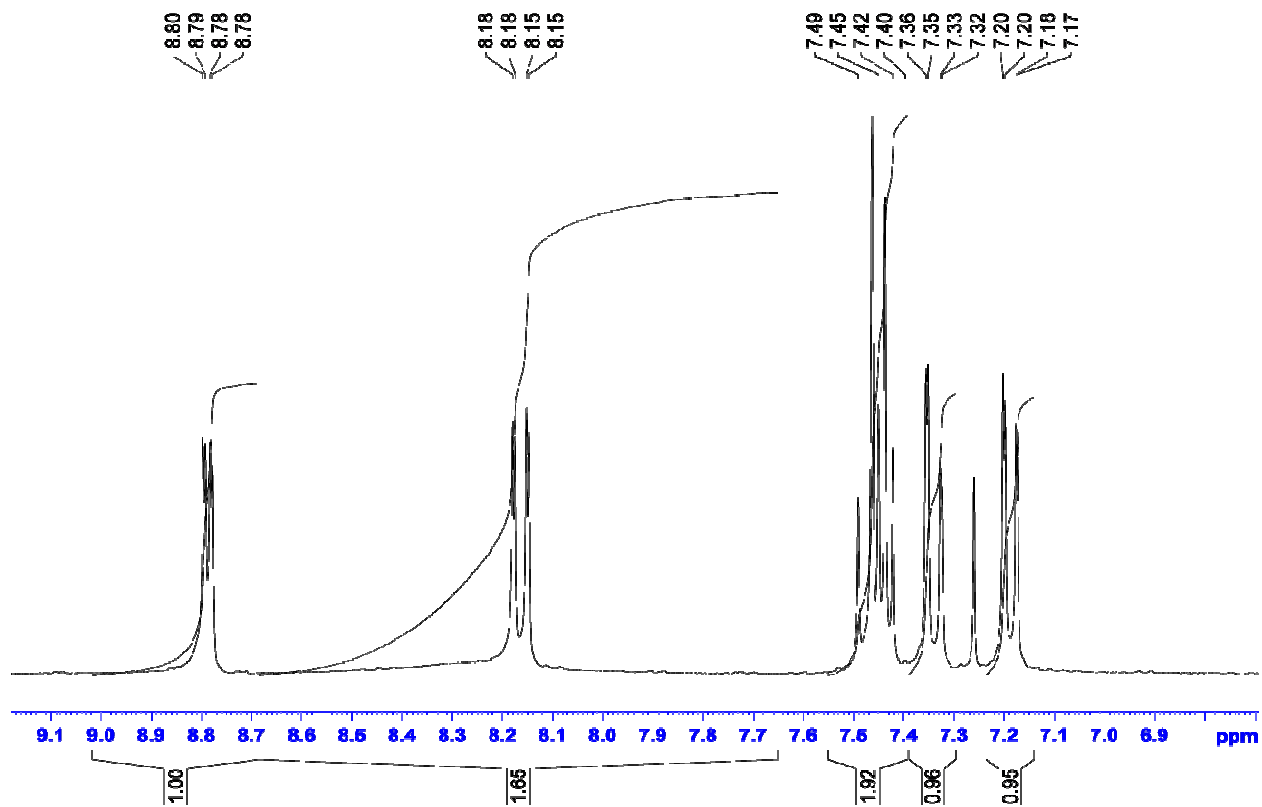


Figure S14 Solution-state ^1H NMR spectrum of $\text{Alq}_3\cdot\text{AcOH-m}$ in CDCl_3 .

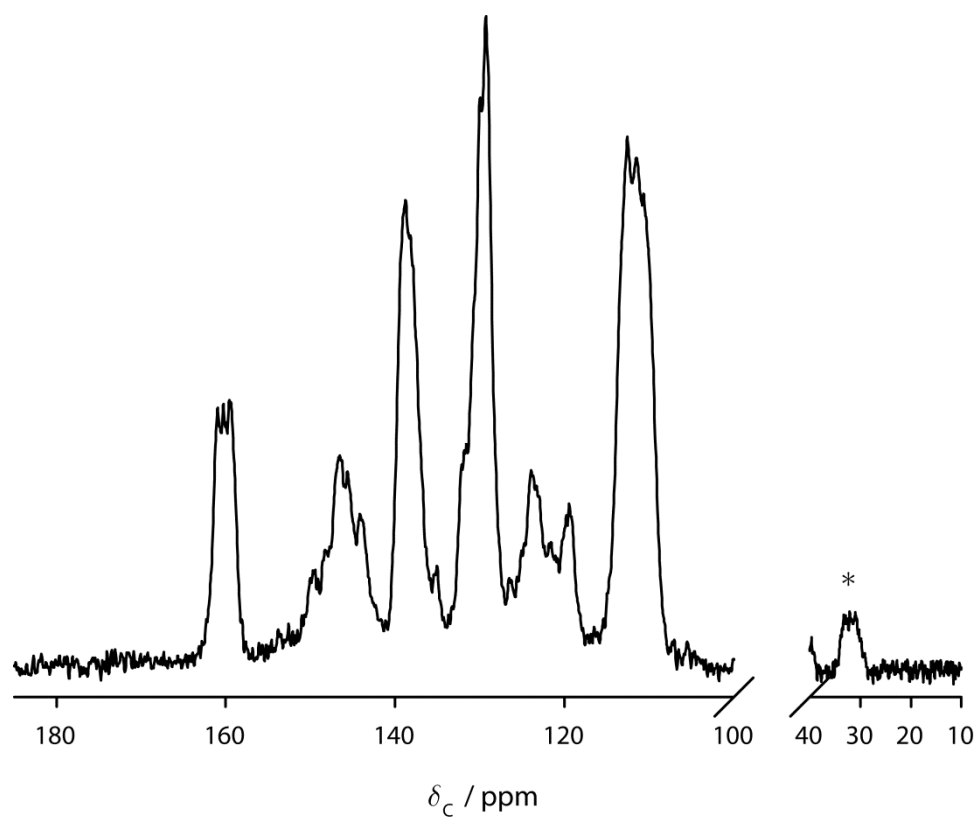


Figure S15 Solid-state ^{13}C CPMAS NMR spectrum of $\text{Alq}_3\text{-m}$ showing significant differences in the aromatic region compared to the solid-state ^{13}C CPMAS NMR spectrum of $\text{Alq}_3\text{-AcOH-m}$ and the absence of peaks due to acetic acid (1592 repetitions, 2 s recycle delay, 1 ms contact time, 8 kHz MAS frequency). Spinning sidebands are indicated by asterisks.

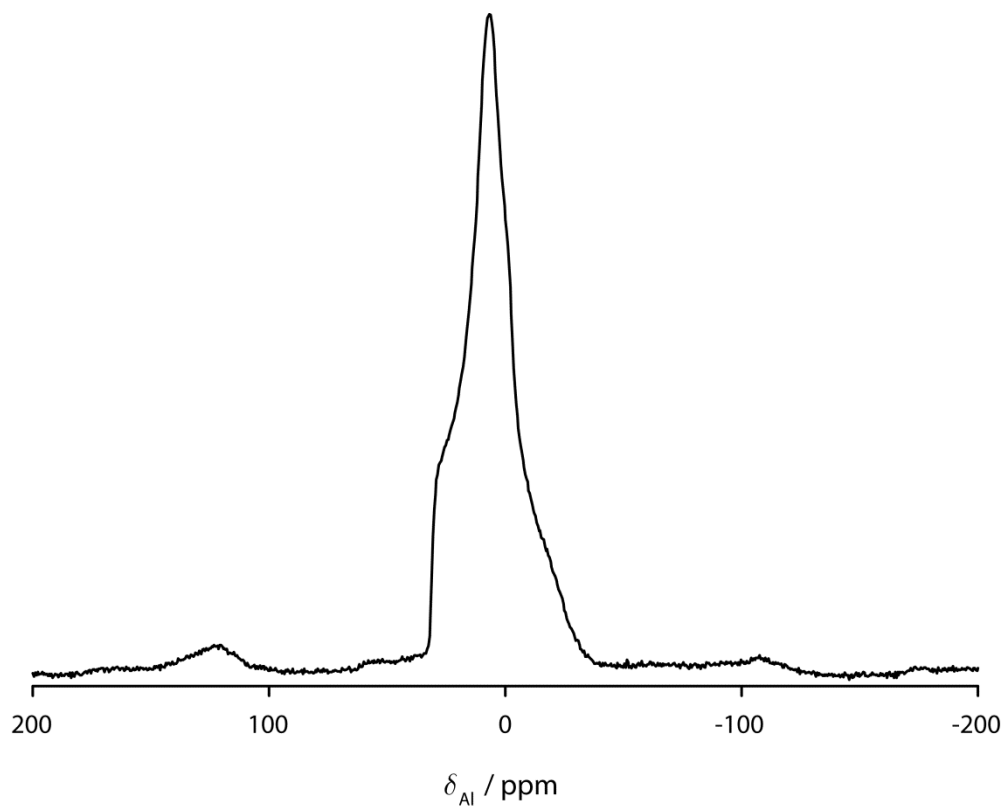


Figure S16 Solid-state ^{27}Al MAS NMR spectrum of $\text{Alq}_3\text{-m}$ (12500 repetitions, 20° pulse, 0.1 s recycle delay, 12 kHz MAS frequency).

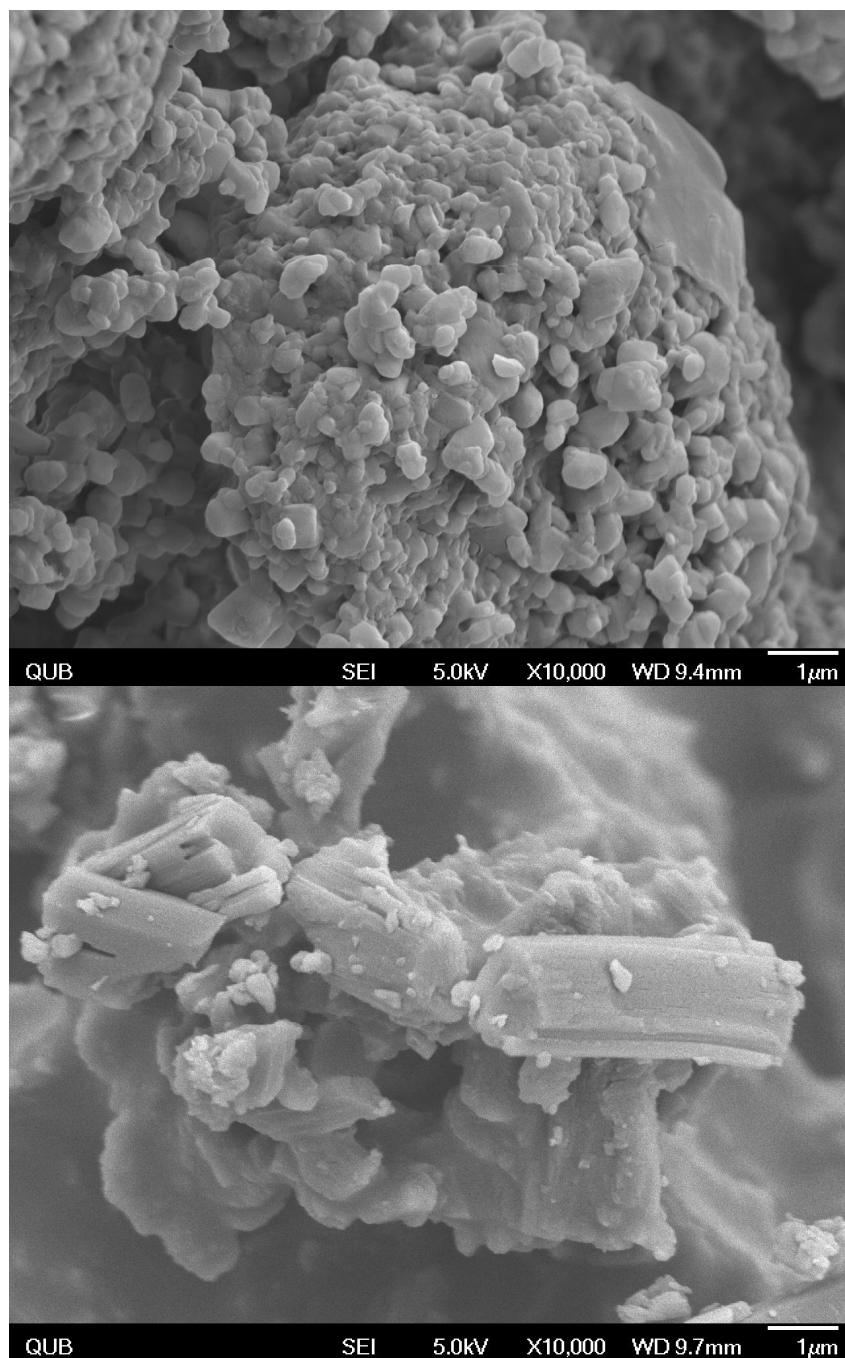


Figure S17 SEM images of Alq₃.AcOH-m (above) and Alq₃-m (below).

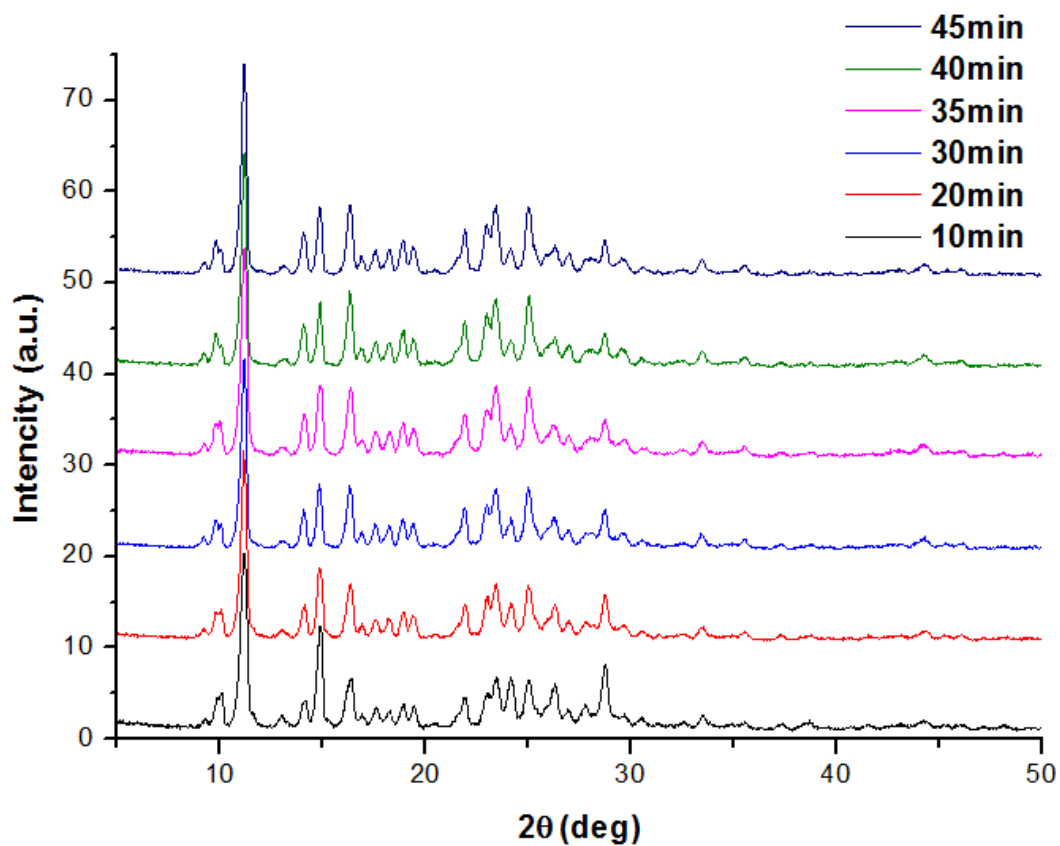


Figure S18 Comparison of powder XRD patterns recorded for the product from the large-scale synthesis of Alq₃.AcOH-m from 10 min to 45 min reaction time.

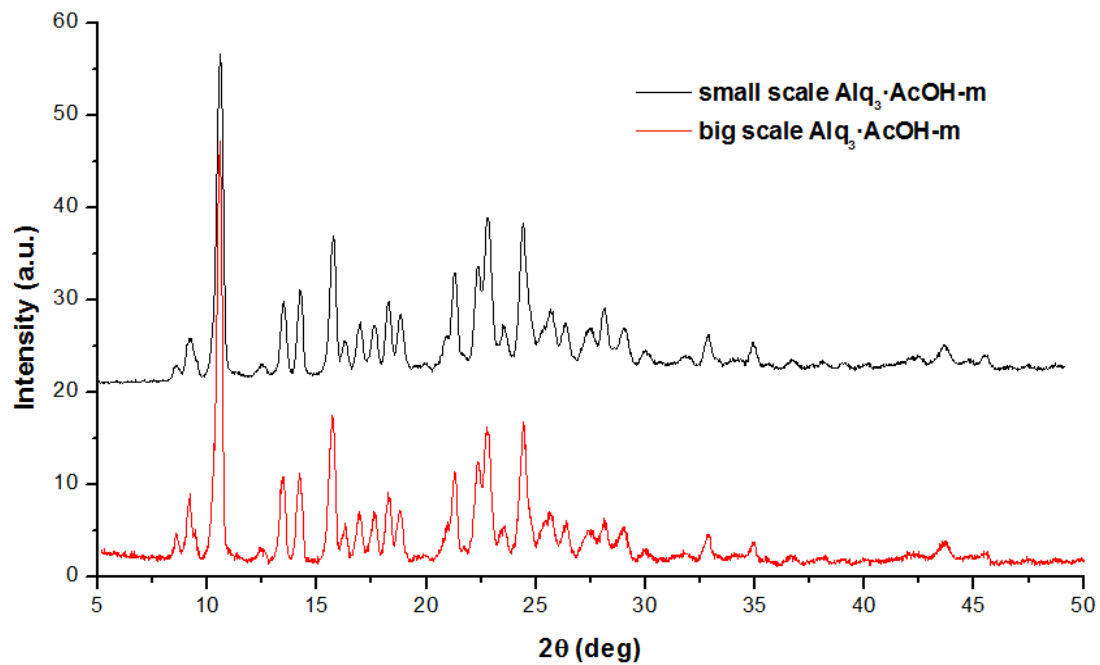


Figure S19 Comparison of experimental powder XRD patterns of $\text{Alq}_3 \cdot \text{AcOH-m}$ obtained from small-scale and large-scale syntheses.

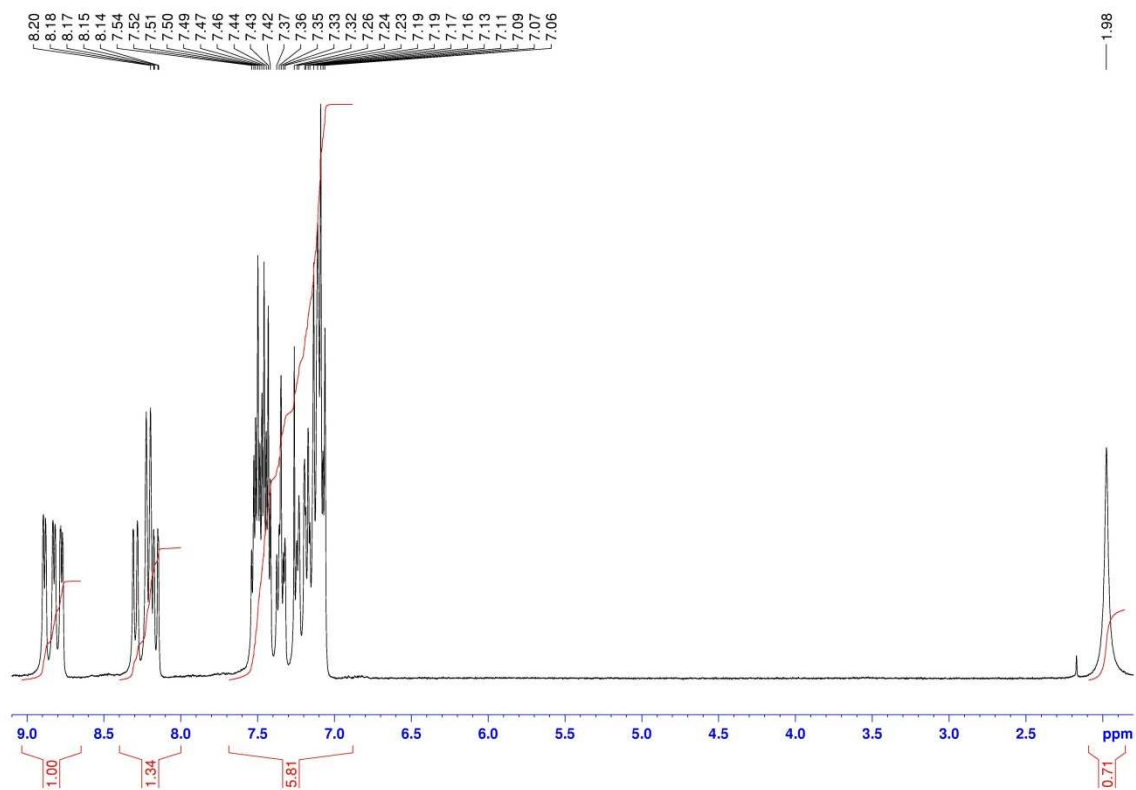


Figure S20 Solution-state ¹H NMR spectrum of Alq₃.AcOH-m obtained from large-scale synthesis.

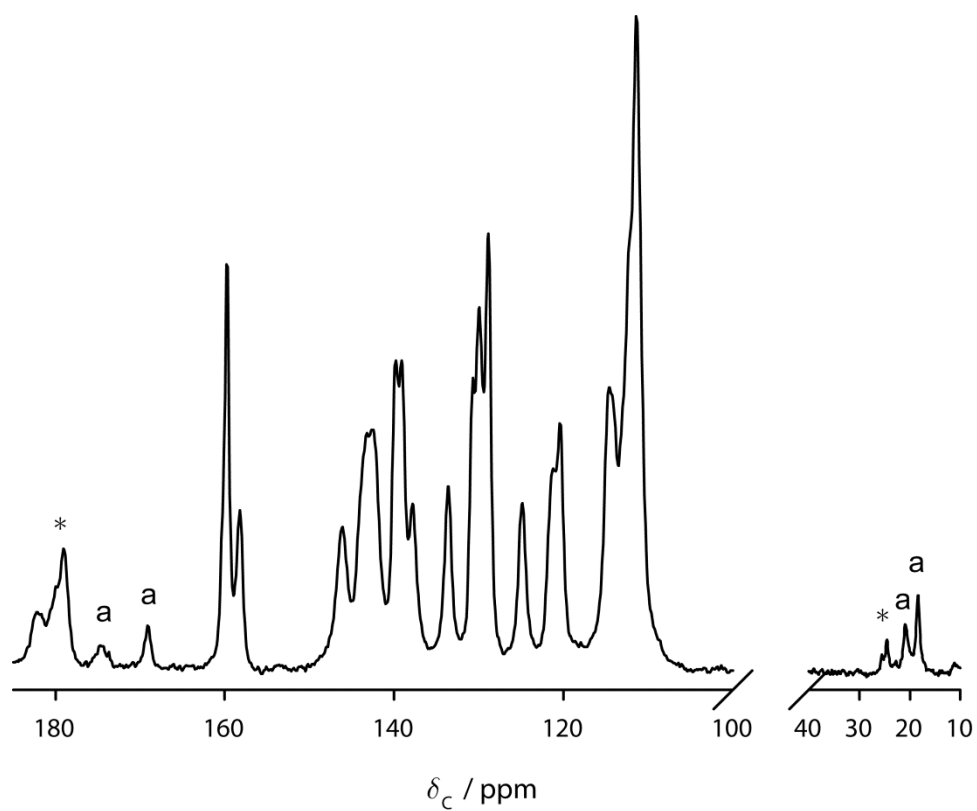


Figure S21 Solid-state ^{13}C CPMAS NMR spectrum of $\text{Alq}_3\cdot\text{AcOH}\cdot\mathbf{m}$ prepared at large scale (532 repetitions, 5 s recycle delay, 1 ms contact time, 6.8 kHz MAS frequency). Peaks due to acetic acid are labeled “a”, and spinning sidebands are indicated by asterisks.

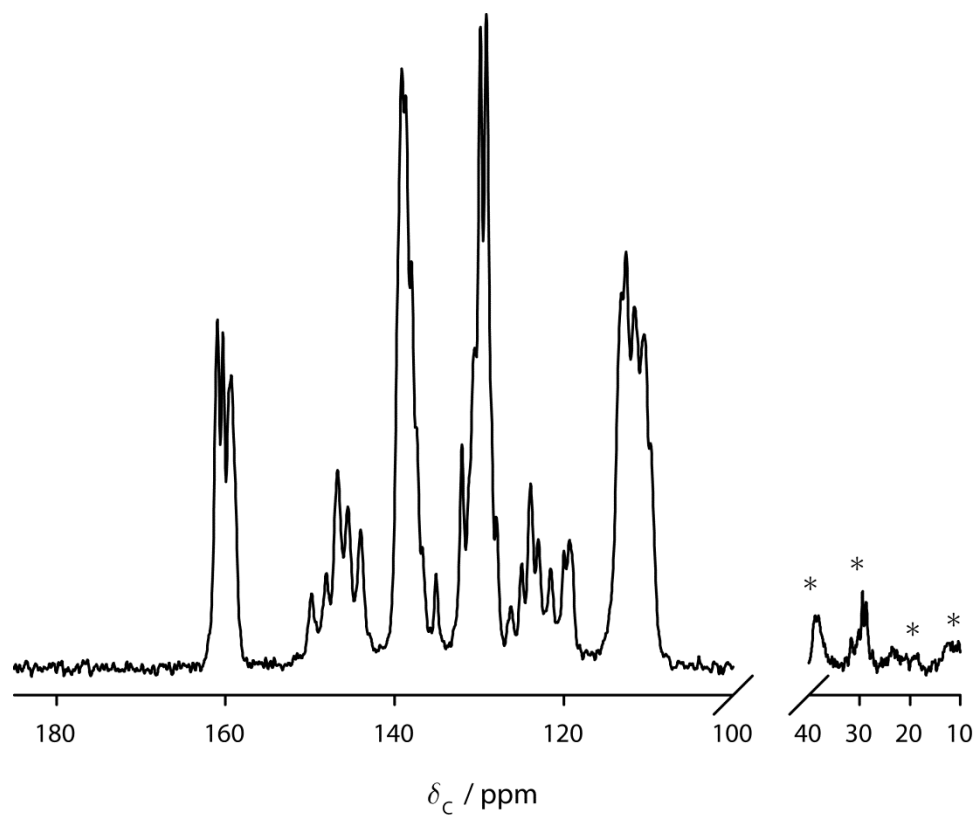


Figure S22 Solid-state ^{13}C CPMAS NMR spectrum of $\text{Alq}_3\text{-m}$ prepared at large scale (376 repetitions, 5 s recycle delay, 10 ms contact time, 10.1 kHz MAS frequency). Spinning sidebands are indicated by asterisks.